Journal of Medicinal Chemistry

Article

Cite This: J. Med. Chem. 2019, 62, 1657−1668

pubs.acs.org/jmc

Antioxidant-Inspired Drug Discovery: Antitumor Metabolite Is Formed in Situ from a Hydroxycinnamic Acid Derivative upon Free-Radical Scavenging

Laura Fási,[†,◆] Florent Di Meo,[‡,◆] Ching-Ying Kuo,[§,◆] Sonja Stojkovic Buric,[∥] Ana Martins,[⊥,††] Norbert Kúsz,[†] Zoltán Béni,[#] Miklós Dékány,[#] György Tibor Balogh,[¶] Milica Pesic,[∥] Hui-Chun Wang,[§] Patrick Trouillas,[‡,▽] and Attila Hunyadi*[,†,○]

[†]Institute of Pharmacognosy, Interdisciplinary Excellence Centre, and [○]Interdisciplinary Centre for Natural Products, University of Szeged, Eötvös str. 6, H-6720 Szeged, Hungary

[‡]INSERM UMR 1248 IPPRITT, Université Limoges, Faculty of Pharmacy, 2 rue du Dr Marcland, F-87000 Limoges, France

[§]Graduate Institute of Natural Products, Kaohsiung Medical University, Shih-Chuan 1st Rd. 100, Kaohsiung 807, Taiwan, ROC

[∥]Department of Neurobiology, Institute for Biological Research, University of Belgrade, Bulevar Despota Stefana 142, 11060 Belgrade, Serbia

[⊥]Institute of Medical Microbiology and Immunobiology, Faculty of Medicine, University of Szeged, Dóm tér 10, H-6720 Szeged, Hungary

[#]Spectroscopic Research and [¶]Compound Profiling Laboratory, Gedeon Richter Plc., Gyömrői u. 19-21, H-1103 Budapest, Hungary

[▽]RCPTM, Faculty of Sciences, Palacký University, tr. 17. listopadu 12, 771 46 Olomouc, Czech Republic

Supporting Information

ABSTRACT: Cancer cells generally possess higher levels of reactive oxygen species than normal cells, and this can serve as a possible therapeutic target. In this proof-of-concept study, an antioxidant-inspired drug discovery strategy was evaluated using a hydroxycinnamic acid derivative. The processing of oxidized mixtures of *p*-coumaric acid methyl ester (**pcm**) revealed a new antitumor lead, graviquinone. Graviquinone bypassed ABCB1-mediated resistance, induced DNA damage in lung carcinoma cells but exerted DNA protective activity in normal keratinocytes, and modulated DNA damage response in MCF-7 cells. The cytotoxic effect of **pcm** in MCF-7 cells was potentiated under H_2O_2-induced oxidative stress, and the formation of graviquinone was confirmed by Fenton's reaction on **pcm**. In silico density functional theory calculations suggested graviquinone as a kinetic product of **pcm**-scavenging $^{\bullet}OH$ radicals. Our results demonstrate the pharmacological value of an in situ-formed, oxidative stress-related metabolite of an antioxidant. This might be of particular importance for designing new strategies for antioxidant-based drug discovery.

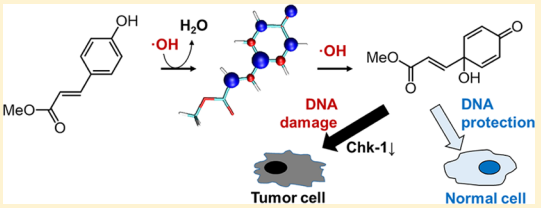

INTRODUCTION

Hydroxycinnamic acids, such as *p*-coumaric, caffeic, ferulic, and chlorogenic acids, are among the most abundant dietary antioxidants. They occur in many vegetables (e.g., olive, potato, lettuce, broccoli, cauliflower, chicory, and cabbage), fruits (e.g., various berries, grapes, dates, and apple), cereals (e.g., common and hard wheat and cereal products such as bread), spices (e.g., clove, Ceylon cinnamon, nutmeg, and cumin), nuts (e.g., peanut), dark chocolate, vegetable oils, and beverages (e.g., beers, wines, fruit juices, tea, and coffee).[1] The antioxidant properties of these phenolic acids have been widely described.[2−4] They have been reported for a large variety of bioactivities, including chemopreventive and antitumor effects. For example, caffeic acid methyl ester (**cm**) was shown to inhibit colon carcinogenesis through the inhibition of tyrosine protein kinase and arachidonic acid metabolism.[5] Another example is the chemopreventive activity of *p*-coumaric acid methyl ester (**pcm**; also referred to as methyl-*p*-coumarate), which is enabled by the induction of phase II metabolic enzymes such as quinone reductase and glutathione-*S*-transferase.[6]

In addition to the antitumor and antioxidant potential of hydroxycinnamic acids, some inspiring studies about their oxidized metabolites have been published. Pieters et al. found that Ag_2O-catalyzed biomimetic oxidation of **cm** or ferulic acid methyl ester (**fm**) in a mixture of anhydrous benzene and anhydrous acetone yielded dihydrobenzofuran lignans with highly potent in vitro antiproliferative activity on different cancer cell lines.[7] The dimer of **cm** showed great antitumor potential with growth inhibitory concentrations (GI_{50}) lower than 10 nM against breast cancer cell lines, MDA-MB-435, MDA-N, and BT-549. Moreover, this compound was identified

Received: December 20, 2018
Published: January 7, 2019

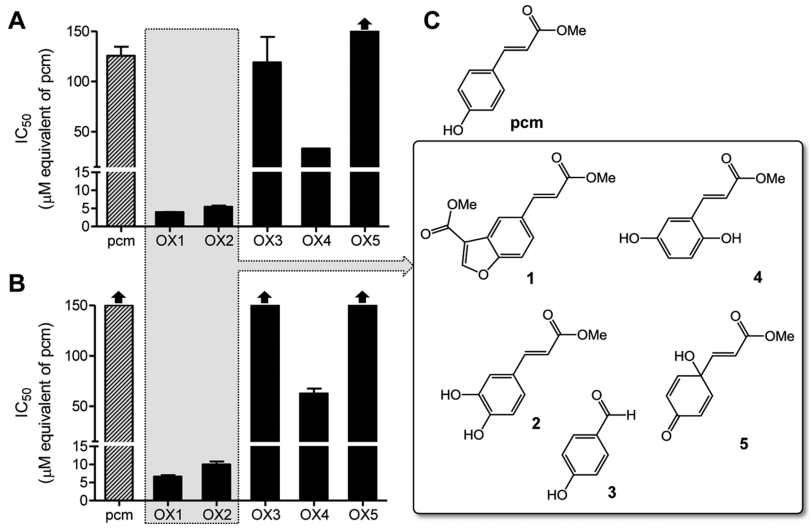

Figure 1. Cytotoxic activity of **pcm** and its oxidized metabolite mixtures OX1-5 on L5178 (A) and L5178$_{B1}$ (B) cancer cells, and chemical structures of **pcm** and its oxidized metabolites isolated (C). Dilutions for each mixture were performed by calculating with the molecular mass of **pcm**; upward arrows mark samples with IC_{50} values >150 μM. Reagents and solvents for obtaining each mixture were as follows. OX1: PIFA, ACN; OX2: PIFA, ACN−water (9:1); OX3: PIFA, MeOH; OX4: PIFA, MeOH−water (9:1), and OX5: PCC, CH_2Cl_2.

as a potent antitubulin agent.[7] These dihydrobenzofuran lignans were also reported to exert antiangiogenic activity,[8] and another study described similar activity of the **fm**-derived lignan on angiogenesis.[9] Recently, the above-mentioned dimer of **cm** (referred to as Q2-3) attracted great attention for its antimetastatic activity on mammary tumors because of the interference with their microenvironment; namely, Q2-3 was able to induce IL-25 secretion from tumor-associated fibroblasts.[10]

As one of the mechanisms preventing free-radical-associated damage, antioxidants can scavenge free radicals. In turn, this process may form oxidized metabolites with different bioactivities. The effect of these metabolites on the overall bioactivity may be minor, or at least difficult to discriminate with respect to that of their parental antioxidants within the cell environment. However, these metabolites could be used as new model compounds or leads in drug discovery. In this context, and considering the intriguing antitumor potential of hydroxycinnamic acids, this study aims at the investigation of both the formation and the bioactivity of oxidized metabolites of **pcm**.

RESULTS AND DISCUSSION

Preparation of Oxidized Metabolites of pcm. As a first step, we aimed to study the effect of various oxidative conditions on the cytotoxic activity of **pcm**. The oxidation of **pcm** was performed by a hypervalent iodine(III) reagent, phenyliodine bis(trifluoroacetate) (PIFA), in acetonitrile (ACN), ACN−water (9:1, v/v), methanol, or methanol−water (9:1, v/v), or with pyridinium chlorochromate (PCC) in dichloromethane. PIFA was selected based on two reasons. First, this reagent was previously reported to react with *p*-phenols via a single-electron transfer (SET) mechanism through a cation radical intermediate.[11] Second, this cation radical intermediate can deprotonate in aqueous medium and lead to the same phenoxyl radical that would form in a hydrogen atom transfer (HAT) reaction. As *p*-coumaric acid was previously suggested to scavenge reactive oxygen species (ROS) either through SET or HAT mechanism,[12] we expected that PIFA-mediated oxidation of **pcm** would lead to a metabolite pattern similar to that of ROS scavenging. Following oxidation, each product mixture was subjected to solid-phase extraction on silica to prevent false-positive results because of residual traces of reagents. The obtained product extracts (named OX1-5) were tested for their cytotoxic activity in comparison with that of **pcm** on a mouse lymphoma cell line (L5178) and its multidrug-resistant (MDR) subcell line, obtained by transfection of L5178 with the human *ABCB1* gene (L5178$_{B1}$). A dramatic increase in the cytotoxic activity was observed with OX1 and OX2 as compared to that of **pcm** (Figure 1A,B); hence, these conditions were chosen to perform scale-up in order to allow the isolation of individual active constituents. Altogether, three scale-up procedures were performed, from which five metabolites (**1**−**5**, see Figure 1C) were isolated by combined chromatographic techniques. Structure elucidation of these compounds was (i) performed by mass spectrometry (MS) and comprehensive one-dimensional (1D) and two-dimensional (2D) nuclear magnetic resonance (NMR) methods and then (ii) confirmed by comparing their chemical shifts with reported literature values.[13−16]

Compound **1** has most likely been formed from **pcm** in a way similar to that previously described for the dihydrobenzofuran dimers of **cm** or **fm**, followed by the elimination of a phenol moiety and the formation of benzofuran skeleton. The formation of compounds **2** (i.e., **cm**) and **3** (*p*-hydroxybenzaldehyde) can intuitively be explained by the impact of the oxidative environment. Compound **4** (methyl 2,5-dihydroxycinnamate or methyl grevillate) represents a highly unexpected structure, which has, however, previously been isolated from natural sources.[16] Considering the reaction mechanism of phenol oxidation by PIFA,[11] one can only suspect the formation and opening-up of an epoxide intermediate as an explanation for the unexpected migration of the *p*-hydroxyl group to the meta-position. Compound **5** (known as graviquinone) is also a natural product that has first been isolated from the "silky oak," *Grevillea robusta* A. Cunn, and identified as a cytotoxic compound against MCF-7, NCI-H460, and SF-268 cell lines in vitro.[15] The *p*-quinol moiety of **5** makes it related to protoflavones that are known for their strong antitumor activity in vitro and in vivo,[17] as well as for their ability

DOI: 10.1021/acs.jmedchem.8b01994
J. Med. Chem. 2019, 62, 1657−1668

to bypass resistance mediated by the P-glycoprotein (P-gp)/ABCB1 or breast cancer resistance protein/ABCG2 efflux transporters.[18]

Antitumor Potential of Oxidized pcm Metabolites. The in vitro cytotoxic activity of compounds **1**−**5** was tested on the above-mentioned mouse lymphoma cell line pair (L5178 and $L5178_{B1}$). Following this, compounds **4** and **5** were also tested on a diverse panel of cancer cell lines, including MCF-7, HeLa, and SiHa, and several lung carcinoma cell lines, such as A549 adenocarcinoma, a highly metastatic large cell lung carcinoma (NCI-H661), and a non-small-cell lung carcinoma (NCI-H460) and its MDR counterpart (NCI-H460/R) developed by continuous exposure of the initially sensitive cell line to doxorubicin. Results of these bioassays are compiled in Table 1.

The parental antioxidant **pcm** exerted very low cytotoxic activity as measured by 3-(4,5-dimethylthiazol-2-yl)-2,5-diphenyltetrazolium bromide (MTT) assay, and the NCI-H460/R cell line showed a nearly 10-fold cross-resistance to this compound as compared to the NCI-H460 cells. Some of its oxidized metabolites, however, exerted a great, ca. 2−3 orders of magnitude stronger cytotoxic activity. Among the two identified active metabolites (**4** and **5**), 2.4 times cross-resistance toward the hydroquinone analogue compound **4** was observed in the MDR cell line $L5178_{B1}$, suggesting that this compound is likely a substrate of the P-gp/ABCB1 efflux transporter. Nevertheless, the resistance profile of this compound was much more favorable than that of **pcm** on the NCI-H460/NCI-H460/R cell line, exhibiting a less than twice cross-resistance in the latter. Compound **5** bypassed resistance of both the ABCB1-transfected cell line and NCI-H460/R adapted to doxorubicin. Its activity was as strong as that of the positive control doxorubicin in L5178 cells, but while doxorubicin demonstrated 28.9 times higher IC_{50} in resistant $L5178_{B1}$ compared to corresponding sensitive L5178 cells, compound **5** was similarly active in both cell lines. Moreover, compound **5** showed a nearly 10 times selective cytotoxicity against the lymphoma cell lines, and a ca. 2−3 times selectivity against the NCI-460 and NCI-661 cell lines versus the immortalized human keratinocytes (HaCaT), suggesting a good selectivity profile toward cancer cells.

Cell death analysis by annexin-V/propidium iodide (PI) staining revealed that both compounds **4** and **5** induce cellular necrosis (Table 2).

Compound **4** exerted the strongest effect on NCI-H460 cells, which were also the most sensitive to **4** according to the cytotoxicity assay. As the most prominent effect, compound **5** increased the percentage of necrotic NCI-H661 cells from 2.58% (untreated control) to 44.82% (treated). This was similar to our previous observations on a *p*-quinol flavonoid, protoapigenone, which also induced necrosis-type cell death associated with ataxia telangiectasia and Rad3-related kinase (ATR) inhibition through Chk1, leading to the accumulation of DNA lesions.[19] Considering the structural relationship between protoapigenone and compound **5**, our attention turned toward its potential ability to exert DNA damage and interfere with DNA damage response (DDR) at the same time.

As a marker of DNA damage, the expression of histone 2A.X (H2A.X) was analyzed after treatment with compound **4** or **5**. The potential effect of compound **5** on DDR was evaluated with western immunoblotting after UV irradiation of MCF7 cells (Figure 2).

The results clearly showed the induction of DNA damage by **5** in NCI-H460 and NCI-H460/R cells with significantly

Table 1. In Vitro Cytotoxic Activity of pcm and Its Oxidized Metabolites 1−5[a]

	IC_{50} ± SEM (μM)									
	L5178	$L5178_{B1}$	NCI-H460	NCI-H460/R	A549	NCI-H661	HaCaT	MCF-7	HeLa	SiHa
pcm	125.60 ± 8.89	>150	120.01 ± 2.14	1043.13 ± 59.36	322.92 ± 8.09	289.21 ± 8.42	311.22 ± 3.75	>400	>150	>150
1	>150	>150								
2	103.9 ± 3.02	112.8 ± 4.45								
3	>150	>150								
4	5.23 ± 0.29	12.38 ± 0.23	3.77 ± 0.07	7.05 ± 0.13	4.14 ± 0.09	4.19 ± 0.11	9.69 ± 0.18		8.51 ± 1.54	
5	0.46 ± 0.09	0.62 ± 0.08	1.85 ± 0.03	2.06 ± 0.03	4.32 ± 0.09	1.44 ± 0.02	4.05 ± 0.10	6.22 ± 1.07	9.85 ± 1.03	8.89 ± 1.09
Dox	0.41 ± 0.07	11.83 ± 0.64	0.04 ± 0.01	1.89 ± 0.25	0.55 ± 0.16	0.35 ± 0.12	0.03 ± 0.01	1.08 ± 0.01	1.21 ± 0.05	0.76 ± 0.01

[a] IC_{50} values are given in μM as mean ± standard error of the mean (SEM) from three parallel experiments; **Dox**: doxorubicin.

DOI: 10.1021/acs.jmedchem.8b01994
J. Med. Chem. 2019, 62, 1657−1668

Table 2. Cell Death Induction by Compounds 4 and 5 in Human Lung Carcinoma Cell Lines (NCI-H460, NCI-H460/R, A549, and NCI-H661) and Normal Human Keratinocytes (HaCaT)[a]

cell line	sample	viable cells	early apoptosis	late apoptosis	necrosis
NCI-H460	control	96.49 ± 0.96	0.45 ± 0.01	0.93 ± 0.04	2.13 ± 0.02
	4	86.64 ± 1.73**	0.34 ± 0.01	5.10 ± 0.15**	9.92 ± 0.20**
	5	89.13 ± 2.67*	0.21 ± 0.01	3.35 ± 0.07**	7.31 ± 0.22**
	Dox	85.14 ± 3.07*	4.05 ± 0.12**	4.11 ± 0.23**	6.70 ± 0.24**
NCI-H460/R	control	95.76 ± 2.87	0.22 ± 0.01	0.84 ± 0.01	3.17 ± 0.13
	4	89.65 ± 1.79*	0.16 ± 0.01	2.48 ± 0.10*	7.71 ± 0.08**
	5	90.03 ± 3.60*	0.12 ± 0.01	2.34 ± 0.07*	7.51 ± 0.15**
A549	control	96.45 ± 2.89	0.48 ± 0.01	1.54 ± 0.03	1.52 ± 0.05
	4	88.24 ± 2.65*	2.36 ± 0.07*	5.62 ± 0.06**	3.78 ± 0.15*
	5	92.78 ± 1.86	0.72 ± 0.03	3.93 ± 0.16*	2.57 ± 0.03*
NCI-H661	control	96.16 ± 0.96	0.31 ± 0.01	0.95 ± 0.03	2.58 ± 0.05
	4	89.43 ± 1.79*	0.49 ± 0.02	3.39 ± 0.07*	6.69 ± 0.20*
	5	45.43 ± 1.36***	0.18 ± 0.01	9.57 ± 0.10***	44.82 ± 1.79***
HaCaT	control	95.63 ± 3.83	0.23 ± 0.01	2.26 ± 0.09	1.88 ± 0.02
	4	90.95 ± 3.64*	0.50 ± 0.01	2.65 ± 0.08	5.90 ± 0.12**
	5	91.50 ± 1.83	0.44 ± 0.01	2.85 ± 0.06	5.21 ± 0.16**
	Dox	78.11 ± 2.38**	11.03 ± 0.14***	3.04 ± 0.07	7.82 ± 0.12***

[a]**Dox**: 40 nM of doxorubicin, used as positive control. Statistical evaluation was performed by two-way ANOVA followed by Dunnett's multiple comparisons test; *: $p < 0.05$, **: $p < 0.01$, ***: $p < 0.001$.

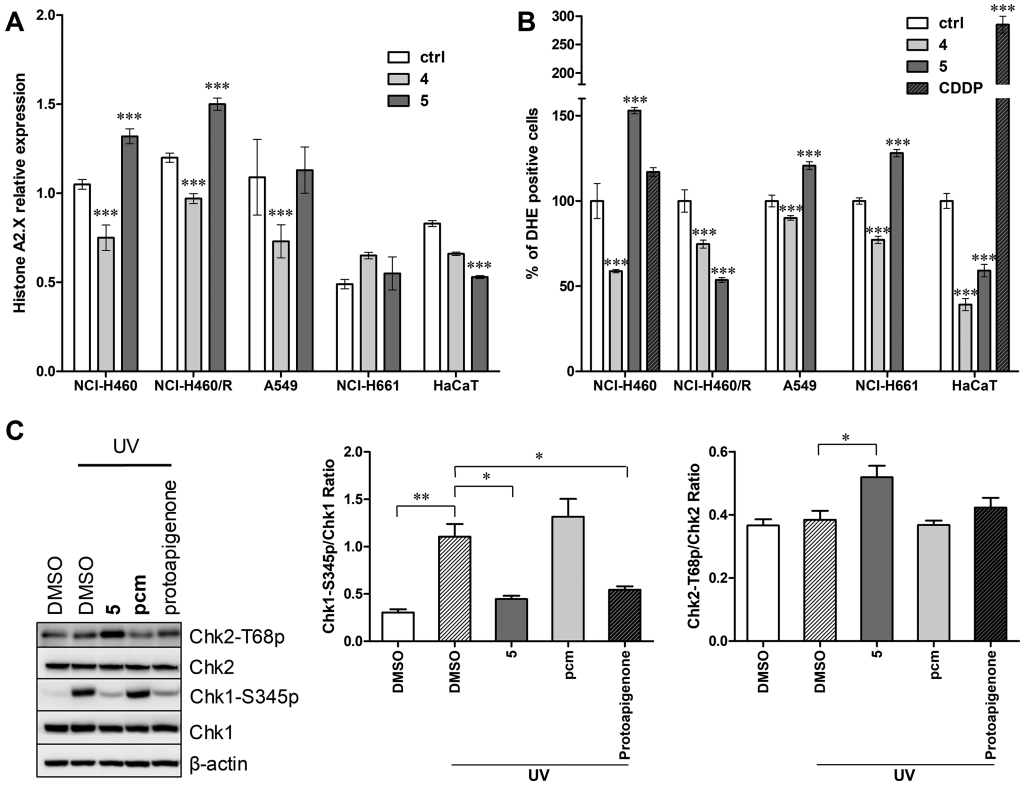

Figure 2. DNA damaging effect and ROS production by treatment with compound **4** or **5** and effect of compound **5** on DDR. (A) DNA damaging effects of compounds **4** and **5** were examined by H2A.X relative expression. (B) ROS production was detected according to dihydroethidium (DHE) fluorescence. Both analyses were performed by flow cytometry, and the results are given as the average ± standard deviation (SD) from three independent experiments. Statistical evaluation was performed by two-way analysis of variance (ANOVA) followed by Dunnett's multiple comparisons test; ***: $p < 0.001$. CDDP: cisplatin. (C) Evaluation of the DNA damaging effect of compound **5** and **pcm** by western immunoblotting; MCF7 cells were pretreated with 10 μM of compound **5** or **pcm** for 30 min and exposed to UV irradiation (10 J/m^2) in the following 1 h to induce DDR. Protoapigenone (10 μM) was used as positive control. Results were analyzed by one-way ANOVA and data represent the mean ± SD from three independent experiments; *: $p < 0.05$, **: $p < 0.01$.

increased expression of H2A.X, which was, however, decreased in normal HaCaT cells after treatment with **5**. The results point out the selectivity of compound **5** toward DNA damaging in cancer cells. Compound **4** reduced the expression of H2A.X in most of the cancer cells and also in HaCaT cells, indicating its DNA protective activity (Figure 2A). ROS production was

DOI: 10.1021/acs.jmedchem.8b01994
J. Med. Chem. 2019, 62, 1657−1668

assessed by DHE labeling that showed a significant increase of ROS levels in NCI-H460, A549, and NCI-H661 cells after treatment with compound **5**; however, it was decreased in NCI-H460/R and HaCaT cells. These results also demonstrate the selectivity of **5** toward cancer cells. The opposite effect on NCI-H460/R cells should be discussed in the light of our previously published results regarding the lower antioxidant potential of NCI-H460/R cells, as compared to that of their parental cell line NCI-H460.[20] Compound **4** decreased the level of ROS in all tested cell lines including HaCaT cells (Figure 2B). The obtained results indicate different mechanisms of action for compounds **4** and **5**. Interestingly, the positive control cisplatin (CDDP) significantly increased ROS levels in normal HaCaT cells without affecting this measure in NCI-H460 cancer cells. This also suggests that, at least in this regard, compound **5** has a better selectivity profile than the classical chemotherapeutic drug cisplatin.

It is of interest that compound **5** acted as a potent modulator of DDR through the inhibition of Chk1-S345 phosphorylation, while **pcm** was completely inactive in this regard (Figure 2C). The serine−threonine checkpoint kinases 1 and 2 (Chk1 and Chk2, respectively) have key roles in the DNA damage signaling response. Upon DNA damage, Chk1 is activated through phosphorylation by ATR, and Chk2 is activated to a major extent by ataxia telangiectasia mutated kinase (ATM). Chk1 is especially important for the stability of stalled replication forks, and DNA repair-defective tumor cells have been shown to accumulate high levels of DNA damage.[21] A growing body of evidence suggests that small-molecule Chk1 inhibitors may act as single agents against cancer cells with specific potential genetic defects, as, for example, Fanconi anemia.[22] In addition, the sensitivity to Chk1 inhibition is also associated with replication stress in many cancer cell types, such as neuroblastoma cell lines or metastatic melanoma, which were found to have higher expression of Chk1 mRNA.[23,24] Accordingly, our results demonstrated that, as a Chk1 inhibitor, compound **5** has a considerable potential to specifically target cancer cells with high levels of endogenous DNA damage. Furthermore, the increased expression of phosphorylated H2A.X is a well-known marker of the DNA double-strand breaks (DSBs).[25] We found that, unlike normal HaCaT cells, cancer cells treated with compound **5** showed a significantly increased expression of H2A.X (Figure 2A). As ATM-dependent phosphorylation is also correlated with H2A.X phosphorylation, this suggests that DSBs resulting from collapsed replication forks are responsible for the ATM activation. In Figure 2C, our results demonstrate that compound **5** can increase Chk2-T68 phosphorylation, suggesting that it could induce DSBs and activate the ATM−Chk2 pathway. This is an interesting difference between compound **5** and the positive control protoapigenone, a *p*-quinol flavonoid, which did not influence the ATM-dependent phosphorylation of Chk2 in accordance with our previous findings.[19]

pcm was reported as a potent dietary antioxidant, counteracting lipid peroxidation in rat liver microsomes with an inhibitory concentration (IC_{50}) value of 0.4 μM.[26] Furthermore, a recently published spectroscopic study on the in vitro antioxidant activity of *p*-coumaric acid indicated that it can efficiently scavenge 2,2-diphenyl-1-picrylhydrazyl, 2,2′-azino-bis(3-ethylbenzothiazoline-6-sulphonic acid), superoxide anion, and H_2O_2, as well as prevent the autoxidation of linoleic acid.[27] As these antioxidant mechanisms are unlikely to be disturbed by the ester function **pcm**, similar activities can reasonably be expected from **pcm** as well. Accordingly, our next aim is to investigate whether or not the identified bioactive metabolites have the chance to form through ROS scavenging by **pcm**. In order to assess this, we studied the $^{\bullet}OH$ radical-scavenging activity of **pcm**.

$^{\bullet}OH$ Radical-Scavenging Activity of pcm. The $^{\bullet}OH$ radical-scavenging capacity of **pcm** was performed by measuring the inhibition of the oxidative damage caused to 2-deoxy-D-ribose by Fenton reaction. A free-radical trapping antioxidant, NXY-059 (disufenton sodium; Cerovive), was used as positive control; this compound reached phase III clinical trials as a neuroprotective agent.[28] We found that **pcm** is a stronger $^{\bullet}OH$ radical scavenger (IC_{50} = 0.345 [95% C.I. 0.313−0.380] mM) in this bioassay than NXY-059 (IC_{50} = 1.826 [95% C.I. 1.501−2.220] mM). The results obtained for NXY-059 were in good agreement with those of our previous study.[29]

In Vitro Antitumor Activity of pcm in the Presence of H_2O_2-Induced Oxidative Stress. MCF-7 cells were subjected to a combined treatment with **pcm** and H_2O_2, aiming to investigate whether or not externally provoked oxidative stress can modulate sensitivity of cells toward **pcm** (Table 3).

Table 3. Interaction between pcm and H_2O_2 Concerning Their Cytotoxicity on MCF7 Cells[a]

H_2O_2 vs **pcm**	CI_{50}	CI_{75}	CI_{90}	D_m	m	r	CI_{avg}
2.5:1	0.79	0.60	0.45	247.66	2.109	0.985	0.556
1.25:1	0.93	0.60	0.39	250.18	3.197	0.988	0.550
0.625:1	1.06	0.68	0.44	222.79	3.610	0.974	0.623

[a]CI values are given at 50, 75, and 90% of cytotoxicity (ED_{50}, ED_{75}, and ED_{90}, respectively). CI_{avg}: weighted average CI value; $CI_{avg} = (CI_{50} + 2CI_{75} + 3CI_{90})/6$. CI < 1, CI = 1, and CI > 1 represent synergism, additivity, and antagonism, respectively. D_m, m, and r represent antilog of the *x*-intercept, slope, and linear correlation coefficient of the median effect plot, respectively.[30] Stability of **pcm** in the presence of H_2O_2 (see Figure S1 in the Supporting Information) suggests that the interaction is not due to a chemical reaction between them.

Synergism could clearly be observed between **pcm** and H_2O_2, particularly at higher rates of inhibition that are more important in terms of antitumor activity.[30] Moreover, there seems to be a tendency in favor of higher H_2O_2 versus **pcm** ratios, further strengthening the assumption that this phenomenon might be connected to the formation of oxidized metabolites of **pcm** proportionally to the level of oxidative stress. It is worth mentioning that **pcm** was found stable for at least 92 h when dissolved in MeOH (1 mg/mL) and 400 μL of hydrogen peroxide (30%) was added [for high-performance liquid chromatography (HPLC)−photometric diode array (PDA) chromatogram, see Supporting Information, Figure S1]. This indicates that the observed increase in the cytotoxic activity is not due to a simple chemical reaction between H_2O_2 and **pcm**.

Fenton Reaction of pcm. With an attempt to model the effect of oxidative stress on **pcm** in terms of providing possible metabolites, **pcm** was subjected to Fenton reaction, which is well-known to provide excess $^{\bullet}OH$ radicals. Following pre-purification with solid phase extraction on silica, the presence of compound **5** was detected in the reaction mixture by reversed-phase-HPLC and HPLC−MS (for the fingerprint chromatograms and LC−MS data, see Supporting Information, Figures S2 and S3). This clearly demonstrates that compound **5** can form when **pcm** scavenges hydroxyl radicals. However, it is worth

DOI: 10.1021/acs.jmedchem.8b01994
J. Med. Chem. 2019, 62, 1657−1668

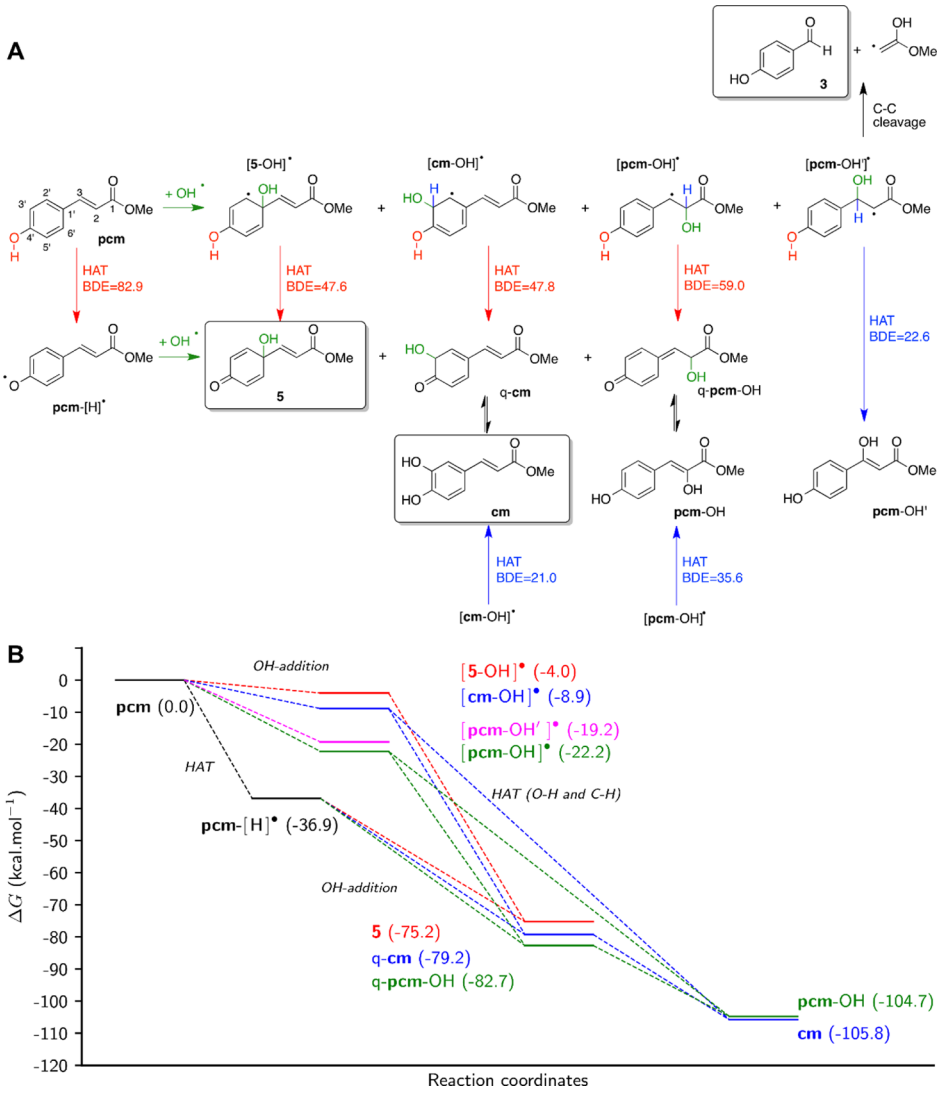

Figure 3. Reactivity of **pcm** in the presence of •OH radical (A) and thermodynamics of the reaction steps (B). HAT: hydrogen atom transfer; q-**pcm** and q-**cm** represent quinone forms of **pcm** and **cm**, respectively. Frames mark species observed experimentally from the Fenton reaction of **pcm** and/or from its oxidation with PIFA. Bond dissociation enthalpy (BDE) is defined as the enthalpy required to the homolytic cleavage of X−H bond as follows: BDE(R−H) = H(R•, 298 K) + H(H•, 298 K) − H(R−H, 298 K), where H is the enthalpy. O−H and C−H BDE values for each HAT are given in red and blue, respectively, in kcal·mol^{-1}. Gibbs energies (ΔG, kcal·mol^{-1}) are indicated for each reaction step relative to that of **pcm**. Evidence for the formation of compound **5** from the Fenton reaction of **pcm** is shown in the Supporting Information, Figures S2 and S3.

mentioning that the extreme oxidative conditions provided by Fenton's reaction do not allow to draw any further quantitative conclusion about the formation of metabolites that could rise in a biological environment when hydroxyl radical (or possibly other types of ROS) scavenging takes place. In order to obtain a deeper insight into the potential relevance of compound **5** formation upon ROS scavenging, in silico studies were performed by means of density functional theory calculations.

In Silico Studies about the Formation of pcm Metabolites in the Presence of •OH Radicals. In the presence of highly reactive species such as •OH free radical, **pcm** may be oxidized following two mechanical sequential chemical pathways (see Figure 3). Mechanism 1 is initiated by •OH addition at various positions, leading to the formation of the corresponding radical adducts that are then stabilized by H-atom abstraction. Mechanism 2 is initiated by H-atom abstraction, forming a radical which then undergoes •OH addition at various positions, forming the corresponding adducts. It is important to note that compound **3** can only be obtained from mechanism 2, whereas compound **5** can be obtained from both mechanisms 1 and 2. A description of these mechanical pathways and the calculated thermodynamic analysis are shown in Figure 3.

Regardless of the mechanism, all predicted compounds are thermodynamically favorable with respect to the parent compound (**pcm**) because every single step exhibits negative Gibbs energies (Figure 3B). The calculated global thermodynamics shows that **cm** and **pcm**−OH are the most favorable compounds (ΔG being −105.8 and −104.7 kcal·mol^{-1}, respectively), while **5** appears much less stable (ΔG = −75.2 kcal·mol^{-1}), which can be easily explained by the loss of aromaticity. It must be stressed that only compounds **5**, **cm**, and **3** were experimentally identified among those that can be formed through the above mechanisms. Therefore, joint experimental observations and calculations suggest the important role of kinetics to allow the formation of the least thermodynamically favorable compounds such as **5**.

DOI: 10.1021/acs.jmedchem.8b01994
J. Med. Chem. 2019, 62, 1657−1668

Mechanism 1. Focus must be given to the OH-addition step, which may occur at several C-atom positions, which drives regioselectivity in the adduct formation. Additions on the aromatic ring, that is, positions C1′ and C3′ (see Figure 3A for numbering of **pcm**) can be predicted by the electronic effect of the OH group at p-position, leading to [**5**−OH]• and [**cm**−OH]•. Such additions are only slightly favorable because of the loss of aromaticity (ΔG being −4.0 and −8.9 for C1′ and C3′ OH-additions, respectively). The higher stability of [**cm**−OH]• as compared to [**5**−OH]• may be explained by the lower geometrical disruption with the side chain while spin density distributions are similar for the two radicals (Figure 4).

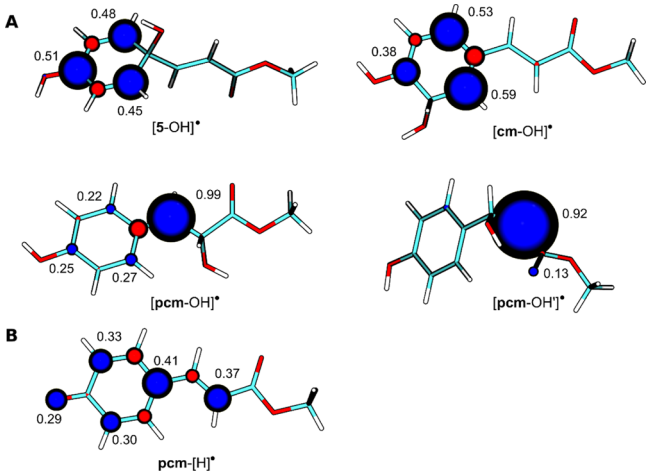

Figure 4. Spin density distribution of the radicals formed by the reaction between **pcm** and •OH radicals. (A) Radicals formed through OH-addition, and (B) radicals formed through hydrogen atom abstraction. Blue and red spheres depict positive and negative atomic spin densities, respectively.

Interestingly, OH-additions at C2 and C3 (leading to [**pcm**−OH]• and [**pcm**−OH′]•) are significantly favored over those taking place at C1′ or C3′. Spin density distributions (Figure 4) in [**pcm**−OH]• and [**pcm**−OH′]• underline the much lower stabilization of single electron with respect to [**5**−OH]• and [**cm**−OH]•. However, the loss of aromaticity is energetically more expensive, which somehow explains the more favorable OH-addition on the C−C double bond than on the aromatic ring. The addition at C2 and thus the formation of [**pcm**−OH]• is the most favorable owing to the slightly more stabilizing delocalization of free radical thanks to the aromatic ring (Figure 4A).

The second step of mechanism 1 is a simple H-atom abstraction driven by the O−H BDEs (see Figure 3A). The lower the BDE, the higher the likelihood of the X−H breaking. It must be stressed that one or two H-atom abstractions may be considered, depending on the adduct. For instance, in [**5**−OH]• and [**pcm**−OH′]•, only OH and C3−H bonds are expected to be broken, respectively. It must be stressed that experimental observations suggest that the C−C bond is broken in [**pcm**−OH′]• allowing rearrangement leading to **3**.

Interestingly, in [**cm**−OH]• and [**pcm**−OH]•, the H-atom may be abstracted from either the phenolic O−H moiety or the C−H bond bearing the new OH-group (i.e., C1′ and C2 for [**cm**−OH]• and [**pcm**−OH]•, respectively). The calculations exhibit very low BDEs (21.0−59.0 kcal·mol^{-1}), suggesting that H-abstraction is not the limiting step of this process. It must be stressed that C−H BDEs of both [**cm**−OH]• and [**pcm**−OH]• are systematically lower than that of O−H, as the former allows turning back to aromatic systems. In the case of OH abstraction, a tautomeric step is required to reach the final products **cm** and **pcm**−OH. However, such event is known to be fast and thermodynamically favorable. Therefore, the observed difference between BDE(O−H) and BDE(C−H) values is not expected to play a crucial role in protic environments.

Mechanism 2. Polyphenols are known to undergo H-atom abstraction from their phenolic OH groups. Here, OH-BDE is −82.9 kcal·mol^{-1} (see Figure 3A), which lies within the typical range of polyphenol BDEs.[31−34] The H-atom abstraction leads to the formation of **pcm**−[H]• free radical that can undergo OH-addition (second step of mechanism 2). In contrast to the OH-addition on **pcm**, this step is more energetically favorable as the products turn back to closed-shell species. The regioselectivity of OH-addition is driven by both thermodynamics and kinetics. On the one hand, thermodynamics suggests that addition preference is at C1′ < C3′ < C2, ΔG being −38.3, −42.4, and −45.8 kcal·mol^{-1} for addition at C1′, C3′, and C2, respectively (see Figure 3B). On the other hand, the kinetics is correlated to the spin density distribution of **pcm**−[H]• (Figure 4). The higher spin density at C1′ suggests that OH-addition at this position is faster, rationalizing the formation of **5**. In other words, calculations suggest that **5** is the kinetic product while q-**cm** and q-**pcm**−OH are the thermodynamic ones. Again, tautomeric steps of q-**cm** and q-**pcm**−OH are not expected to play a key role in the global view of such mechanical pathways.

Competition between Mechanisms 1 and 2. Interestingly, the competition between mechanisms 1 and 2 is a matter of competition between H-atom abstraction and OH-addition on **pcm**. Thermodynamically, H-atom abstraction from *p*-OH (ΔG = −36.9 kcal·mol^{-1}, Figure 3B) is more favorable than OH-addition at any possible position by at least −14.7 kcal·mol^{-1}. Therefore, the major pathway likely starts with H-atom abstraction (mechanism 2). Moreover, this explains the experimentally observed formation of **cm** and **5**; the former being the global thermodynamic product while the latter is a kinetic product from the OH-addition step. It is important to note that the experimental observation of **3** as a product again suggests the importance of kinetics. Such a product can be formed only via the alternative mechanism 1, that is, OH-addition at C2 and thus via [**pcm**−OH′]•. The •OH radical is known to be very reactive and nonspecific, also highlighting certain stochasticity in the reactivity. However, it must be stressed that the higher Gibbs energies of OH-addition at C1′ and C3′ suggest that OH-addition on the aromatic ring is very unlikely.

It must be noted that although theoretical calculations suggest **cm** as a major product, it has only been observed from the PIFA-mediated oxidation and not from the Fenton reaction of **pcm**. This can likely be explained by the fact that the catechol moiety of **cm** might make it particularly sensitive to further oxidation, leading to a rapid decomposition and consequential difficulties of detection under the harsh experimental conditions represented by the Fenton reaction. In addition to this, the presence of an alternative product **4** cannot be fully explained by the proposed mechanism. One can only suspect the formation of an epoxide intermediate and subsequent ring opening as an explanation of the migration of the *p*-hydroxyl group resulting in the hydroquinone derivative **4**.

DOI: 10.1021/acs.jmedchem.8b01994
J. Med. Chem. 2019, 62, 1657−1668

CONCLUSIONS

By processing various oxidized mixtures of **pcm**, two active metabolites were identified from mixtures with the highest antitumor potential. In particular, compound **5** (graviquinone) was revealed as a prospective lead compound, with an ability to bypass multidrug resistance mediated by the ABCB1 transporter, in a lymphoma cell line transfected with ABCB1 gene and an MDR non-small-cell lung cancer cell line established after continuous exposure to doxorubicin. Compound **5** showed a remarkable selectivity toward cancer cells in respect to DNA damage induction. DNA damaging activity of compound **5** was accompanied by its ability to interfere with components of the ATR signaling pathway.

Concerning the possible biological role of compound **5**, our in vitro and in silico studies strongly suggest that it can be formed as a kinetic product when its parental antioxidant, **pcm**, scavenges ROS. The mild in vitro antitumor effect of **pcm** was significantly increased in the presence of H_2O_2-induced oxidative stress, and Fenton's reaction clearly confirmed that the formation of compound **5** from **pcm** is possible upon $^{\bullet}OH$ radical scavenging. Our results provide indirect evidence for the transformation of **pcm** to compound **5** in a biological system facing oxidative stress. The herein described phenomenon also suggests that the oxidative stress-related metabolites of antioxidants represent a segment of chemical space that is rich in valuable bioactive compounds. This would warrant systematic studies on such metabolites as a possible novel drug discovery strategy.

EXPERIMENTAL SECTION

Chromatography. Analytical HPLC was performed on a gradient system of two PU-2080 pumps connected to an MD-2010 Plus photodiode array detector (Jasco Analytical Instruments, Tokyo, Japan), on a Kinetex XB-C18 (5 μm, 100 Å, 250 × 4.6 mm) column with solvent system 1. Semipreparative HPLC was performed on a system of two Waters 600 pumps connected to a Waters 600 2λ detector (Waters, Milford, Massachusetts, USA), on a Kinetex XB-C18 (5 μm, 100 Å, AX, 250 × 21.2 mm) column. HPLC−MS analysis was performed on an Agilent 1200 liquid chromatography system, including a binary pump, a column temperature controller, and a diode array detector (DAD), connected to a 6410 triple quadrupole mass spectrometer (QQQ-MS) equipped with an electrospray ionization (ESI) source (Agilent Technologies, Palo Alto, CA, USA). The analysis was carried out at 45 °C on a Kinetex EVO C18 (2.6 μm, 50 × 3.0 mm, Phenomenex) column with solvent system 2 at a flow rate of 1.25 mL/min.

Solvent system 1: gradient of ACN—from 30 to 70% in water at 0−12 min, 70% of ACN at 12−14 min, then back to 30% of ACN, and the total running time was 25 min.

Solvent system 2: gradient of 2−100% B at 0−5.9 min, 100% of B at 5.9−7.0, from 7.01 min back to 2% of B. Eluent A was 0.1% (v/v) trifluoroacetic acid (TFA) in water, and eluent B was 0.1% TFA in the mixture of ACN−water (95:5).

Flash chromatography was performed on CombiFlash Rf+ (Teledyne ISCO) with **Solvent system 3**: a gradient of ethyl acetate from 0 to 100% in *n*-hexane.

Oxidation of pcm for Screening. As a preliminary experiment, **pcm** was oxidized under different conditions. **pcm** (10.0 mg) was dissolved in 10 mL of ACN (OX1), ACN−water (9:1, v/v) (OX2), MeOH (OX3), MeOH−water (9:1, v/v) (OX4), or dichloromethane (OX5). A quantity of PIFA (48.3 mg, 2 equiv) (OX1-4) or PCC (18.1 mg, 1.5 equiv) (OX5) was added. The reactions were monitored by thin-layer chromatography (TLC) and stopped after 1−4 h, evaporated under vacuum, adsorbed onto 2.0 g of silica, layered on the top of 2.5 g of silica, eluted with 100 mL of EtOAc, and evaporated under vacuum. Each reaction mixture was redissolved in MeOH and analyzed by HPLC, using solvent system 1 at a flow rate of 1 mL/min.

Scale-Up Oxidations I and II. The starting material **pcm** [500 mg (**A**), 200 mg (**B**)] was dissolved in anhydrous ACN [50 mL (**A**)], or in ACN−water [9:1, v/v, 10 mL (**B**)], and a quantity of PIFA [2 equiv, 2413.3 mg (**A**), 965.3 mg (**B**)] was added to the solutions with continuous stirring and heating on 60 °C (**A**). After 5 h (**A**), or 8 h (**B**), the reaction mixtures were evaporated, redissolved in MeOH, and adsorbed onto 12 g of silica. The reaction mixtures were purified by flash chromatography (CombiFlash Rf+) on a silica column (RediSep, 24 g), using a dry-loading technique and solvent system 3 at a flow rate of 35 mL/min. During the purifying process, 233 fractions (**A**) and 177 fractions (**B**) were collected and combined based on their TLC fingerprints. Fractions 46 to 52 (**A**) gave compound **1** in pure form (19.8 mg). From fractions 109 to 116 (**A**), compound **2** was purified with the help of preparative HPLC, using an isocratic elution (45% ACN), detected on 320 nm, and 5.0 mg was obtained. From fractions 57 to 65 (**B**), compound **3** was purified with the help of preparative HPLC, using an isocratic elution (28% ACN), detected on 280 nm, and 6.0 mg was obtained. From fractions 88 to 98 (**B**), compound **4** was purified with the help of preparative HPLC, using an isocratic elution (30% ACN), detected on 280 nm, and 18.9 mg was obtained. All the purified compounds (**1**−**4**) were analyzed by HPLC to check their purity.

Scale-Up Oxidation III. An initial attempt for obtaining compound **5** from **pcm** (200 mg in 200 mL of ACN) by using 2 equiv of PIFA led to an isolated yield as low as 2.43% after purification with flash chromatography and subsequent HPLC. With an aim to increase the yield, the oxidation was repeated with phenyliodine diacetate (PIDA) as follows. After dissolving **pcm** (200 mg) in ACN−water (9:1, v/v, 200 mL), PIDA (723.0 mg, 2 equiv) was added to the solution with continuous stirring. After 1 h, the reaction was stopped, evaporated under vacuum, and adsorbed onto 3.0 g of Celite 545. The reaction mixture was processed through flash chromatography on a silica column (RediSep Gold, 12 g), using dry-loading technique and solvent system 3 at a flow rate of 30 mL/min. Ninety-five fractions were collected and combined based on their TLC fingerprints. Compound **5** was purified from fractions 50 to 55 with preparative HPLC (isocratic elution with 42% aqueous ACN), and 43 mg (yield 19.73%) was obtained.

Compound Characterization Data. Compounds **1**−**5** possessed a purity of >95% by means of HPLC−DAD.

High-resolution MS (HRMS) and MS−MS analyses were performed on a Thermo Velos Pro Orbitrap Elite (Thermo Fisher Scientific) system. The ionization method was ESI operated in positive ion mode. The protonated molecular ion peaks were fragmented by CID at a normalized collision energy of 35%. For the CID experiment, helium was used as the collision gas. The samples were dissolved in methanol. The protonated molecular ion peaks were fragmented by CID at a normalized collision energy of 35%. Data acquisition and analysis were accomplished with Xcalibur software version 2.0 (Thermo Fisher Scientific).

NMR spectra of compounds **1**, **2**, **3**, and **5** were recorded on a Bruker Avance NEO 500 MHz spectrometer equipped with a Prodigy BBO 5 mm CryoProbe. Compounds **1**, **2**, and **5** were dissolved in acetone-d_6, and methanol-d_4 was used for **3** (VWR Chemicals, Belgium). Standard 1D and 2D spectra were processed with MestReNova v6.0.2-5475 software.

NMR spectra of compound **4** were recorded at 25 °C on a Varian 800 MHz spectrometer equipped with a ^{13}C sensitivity-enhanced salt tolerant $^{1}H/^{13}C/^{15}N$ cryogenically cooled probe head. The sample was dissolved in methanol-d_4 (Eurisotop, France). Standard 1D and 2D spectra were acquired using pulse sequences available in the VNMJ 3.2 library. Chemical shifts are reported in the delta scale using residual solvent signals (methanol-d_4: 3.31 or 49.15 ppm, acetone-d_6: 2.05 or 29.84 for ^{1}H or ^{13}C, respectively) as references. For spectral analysis and data reporting, the ACD/NMR Workbook 2015.2.9. software suite (ACD/Labs, Canada) was used.

Compound ***1***. ^{1}H NMR (500 MHz, acetone-d_6): δ 8.56 (1H, s, H-2), 8.28 (1H, d, J = 1.4 Hz, H-4), 7.82 (1H, d, J = 16.1 Hz, H-9), 7.79

DOI: 10.1021/acs.jmedchem.8b01994
J. Med. Chem. 2019, 62, 1657−1668

(1H, dd, J = 8.7, 1.4 Hz, H-6), 7.68 (1H, d, J = 8.7 Hz, H-7), 6.58 (1H, d, J = 16.1 Hz, H-10), 3.94 (3H, s, 8-OCH_3), 3.77 (3H, s, 11-OCH_3); ^{13}C NMR (125 MHz, acetone-d_6): δ 167.5 (C-11), 163.7 (C-8), 157.4 (C-7a), 153.4 (C-2), 145.2 (C-9), 132.0 (C-5), 126.3 (C-6), 126.2 (C-3a), 123.0 (C-4), 118.6 (C-10), 115.4 (C-3), 113.3 (C-7), 52.0 (8-OCH_3), 51.8 (11-OCH_3). HRMS: M + H = 261.07572 (δ = −0.1 ppm; $C_{14}H_{13}O_5$). HR-ESI-MS-MS (CID = 35%; rel. int. %): 247(2); 229(100); 215(7); 197(3).

Compound **2**. ^{1}H NMR (500 MHz, acetone-d_6): δ 7.53 (1H, d, J = 15.9 Hz, H-3), 7.15 (1H, br s, H-5), 7.04 (1H, dd, J = 8.2, 1.2 Hz, H-9), 6.86 (1H, d, J = 8.2 Hz, H-8), 6.27 (1H, d, J = 15.9 Hz, H-2), 3.71 (3H, s, 1-OCH_3). HRMS: M + H = 195.06520 (δ = 0.1 ppm; $C_{10}H_{11}O_4$). HR-ESI-MS-MS (CID = 35%; rel. int. %): 167(15); 163(100); 153(11); 138(25).

Compound **3**. ^{1}H NMR (500 MHz, methanol-d_4): δ 9.76 (1H, s, H-7), 7.76 (2H, d, J = 8.6 Hz, H-2, H-6), 6.91 (2H, d, J = 8.6 Hz, H-3, H-5); ^{13}C NMR (125 MHz, methanol-d_4): δ 192.8 (C-7), 165.2 (C-4), 133.4 (C-2, C-6), 130.3 (C-1), 116.9 (C-3, C-5). HRMS: M + H = 123.04399 (δ = −0.5 ppm; $C_7H_7O_2$). HR-ESI-MS-MS (CID = 35%; rel. int. %): 95(100).

Compound **4**. ^{1}H NMR (800 MHz, methanol-d_4): δ 7.93 (1H, d, J = 16.2 Hz, H-3), 6.90 (1H, d, J = 2.6 Hz, H-9), 6.66−6.74 (2H, m, H-6, H-7), 6.49 (1H, d, J = 16.1 Hz, H-2), 3.77 (3H, s, OCH_3); ^{13}C NMR (201 MHz, methanol-d_4): δ 170.0 (C-1), 151.7 (C-5), 151.4 (C-8), 142.3 (C-3), 122.9 (C-4), 120.4 (C-7), 118.0 (C-2), 117.8 (C-6), 114.8 (C-9), 52.2 (OCH_3). HRMS: M + H = 195.06522 (δ = 0.04 ppm; $C_{10}H_{11}O_4$). HR-ESI-MS-MS (CID = 35%; rel. int. %): 167(3); 163(100); 153(9); 138(1).

Compound **5**. ^{1}H NMR (500 MHz, acetone-d_6): δ 6.85 (2H, d, J = 10.0 Hz, H-3, H-5), 6.68 (1H, d, J = 15.7 Hz, H-7), 6.23 (1H, d, J = 15.7 Hz, H-8), 6.16 (2H, d, J = 10.0 Hz, H-2, H-6), 3.70 (3H, s, 9-OCH_3). HRMS: M + H = 195.06512 (δ = −0.07 ppm; $C_{10}H_{11}O_4$). HR-ESI-MS-MS (CID = 35%; rel. int. %): 181(5); 167(30); 163(100); 153(9); 135(15); 107(5).

Chemicals. RPMI 1640 medium, Dulbecco's modified Eagle's medium (DMEM), fetal bovine serum (FBS), antibiotic−antimycotic solution, penicillin−streptomycin solution, L-glutamine, and trypsin/ethylenediaminetetraacetic acid (EDTA) were purchased from Bioind, Beit Haemek, Israel. MTT was purchased from Sigma, St. Louis, MO, USA. Dimethyl sulfoxide (DMSO) was obtained from Sigma-Aldrich Chemie Gmbh, Germany. The annexin-V-FITC (AV) apoptosis detection kit with PI was purchased from Abcam, Cambridge, UK. DHE was obtained from Molecular Probes, Invitrogen, USA. Phospho-histone H2A.X antibody and secondary antibody Alexa Fluor 488 goat anti-rabbit IgG (H + L) were purchased from Cell Signaling Technology Inc. (Danvers, Massachusetts, USA). Doxorubicin solution was obtained from Ebewe Arzneimittel GmbH. CDDP was obtained from Pfizer (Perth) Pty Ltd. Both drugs were diluted in sterile water prior treatment.

Cells and Cell Culture. Two mouse lymphoma cell lines were used: L5178 mouse T-cell lymphoma cells (ECACC catalog number 87111908, U.S. FDA, Silver Spring, MD, U.S.) and an MDR ($L5178_{B1}$) cell line derived from L5178 by transfection with pHa MDR1/A retrovirus.[35] Cells were cultured in McCoy's 5A media supplemented with nystatin, L-glutamine, penicillin, streptomycin, and inactivated horse serum, at 37 °C and 5% CO_2. $L5178_{B1}$ cell line was selected by culturing the infected cells with 60 μg/L of colchicine (Sigma).

NCI-H460, A549, NCI-H661, and SiHa cell lines were purchased from the American Type Culture Collection, Rockville, MD. HaCaT cell line was obtained from CLS-Cell Lines Service, Eppelheim, Germany. NCI-H460/R cells were selected originally from NCI-H460 cells after 3 months of doxorubicin selective pressure.[36] The HeLa and MCF-7 cell lines were purchased from Bioresource Collection and Research Center, BCRC, Taiwan.

NCI-H460, NCI-H460/R, A549, and NCI-H661 cell lines were maintained in RPMI 1640 medium supplemented with 10% FBS, 2 mM L-glutamine, 10 000 U/mL of penicillin, 10 mg/mL of streptomycin, and 25 μg/mL of amphotericin B solution, while HaCaT cells were cultured in DMEM supplemented with 10% FBS, 2 mM L-glutamine, 4.5 g/L of glucose, 5000 U/mL of penicillin, and 5 mg/mL of streptomycin solution at 37 °C in a humidified 5% CO_2 atmosphere. All adherent cell lines were subcultured at 72 h intervals using 0.25% trypsin/EDTA and seeded into a fresh medium at the following densities: 8000 cells/cm^2 for NCI-H460, NCI-H460/R, and HaCaT and 16 000 cells/cm^2 for H661. MCF-7, HeLa, and SiHa cell lines were maintained in DMEM (Sigma-Aldrich) supplemented with 10% FBS, L-glutamine, and 4500 mg/L of glucose. These cells were cultured at 37 °C in a humidified 5% CO_2 incubator (NuAire).

Cytotoxicity by MTT Assay. Cell viability was assessed by MTT assay.[37] In the case of L5178 and $L5178_{B1}$ cell lines, 6×10^3 cells were added into 96-well flat-bottom microtiter plates, treated with the samples, and incubated for 72 h. Adherent cells grown in 25 cm^2 tissue flasks were trypsinized, seeded into flat-bottomed 96-well tissue culture plates (1000 cells/well for the NCI-H460, NCI-H460/R, A549, and HaCaT cell lines, 2000 cells/well for the NCI-H661 cell line), and incubated overnight in 100 μL of the appropriate medium. After 24 h, the cells were treated with compound **4** (1−20 μM) or **5** (1−20 μM) and incubated for 72 h.

At the end of the incubation period, MTT was added to each well in a final concentration of 0.2 mg/mL for 4 h, as described previously.[20] Formazan product was extracted from cells by DMSO, and the absorbance was measured at 540 nm using an automatic microplate reader (LKB 5060-006 Micro Plate Reader, Vienna, Austria). The values obtained for samples treated with **4** and **5** were corrected with those of blank samples treated with the compounds' solvent DMSO at a maximal concentration of 1.5% v/v. IC_{50} values were defined as the concentration of the drug that inhibited cell growth by 50% and calculated by nonlinear regression analysis using GraphPad Prism 6. For calculated IC_{50} values, see Table 1.

Cell Death Analysis. The percentages of apoptotic, necrotic, and viable cells were determined by AV/PI labeling. All cell lines were incubated overnight in adherent six-well plates (100 000 cells per well for NCI-H460, NCI-H460/R, A549, and HaCaT cell lines, 200 000 cells per well for NCI-H661 cell line) and then subjected to single treatments with 10 μM compound **4** or compound **5**. Treatment with 40 nM doxorubicin was used as positive control in NCI-H460 and HaCaT cells. After 24 h, total (attached and floating) cells were collected. The cell pellet was resuspended in 50 μL of binding buffer containing AV and PI in a ratio of 1:1 (v/v). After the incubation period (10 min at room temperature in the dark), 1 mL of phosphate-buffered saline (PBS) was added and AV/PI staining was analyzed within 1 h by flow cytometry.

The fluorescence intensity of AV (FL1-H channel) and PI (FL2-H channel) was measured on a CyFlow Space flow cytometer (Partec, Münster, Germany). A minimum of 10 000 events were assayed for each sample. Percentages of viable (AV− PI−), early apoptotic (AV+ PI−), apoptotic, and necrotic (AV+ PI+) and dead (AV− PI+) cells were analyzed.

Flow Cytometry. All cell lines were incubated overnight in adherent six-well plates (100 000 cells per well for NCI-H460, NCI-H460/R, A549, and HaCaT cell lines, 200 000 cells per well for NCI-H661 cell line) and then subjected to single treatments with 10 μM compound **4** or **5** that lasted 24 h. Treatment with 2 μM CDDP was used as positive control.

To detect double-strand DNA breaks, cells were labeled with phospho-histone H2A.X (Ser139) antibody coupled with secondary antibody Alexa Fluor 488 goat anti-rabbit IgG (H + L). Adherent cells were harvested by trypsinization, washed twice in PBS, and fixed in 4% paraformaldehyde for 10 min at room temperature. Cells were then permeabilized by adding ice-cold 90% methanol and stored at −20 °C overnight. After washing in PBS, cells were blocked for 60 min with 0.5% bovine serum albumin in PBS. Cells were then resuspended in 100 μL of primary antibody diluted in 0.5% bovine serum albumin (1:1000) and incubated for 60 min at room temperature. After washing in PBS, cells were resuspended in 100 μL of secondary antibody (1:1000) and incubated for 30 min at room temperature.

To detect ROS level, cells were stained with superoxide indicator DHE. Adherent cells were harvested by trypsinization and incubated in medium with 1 mM DHE for 30 min at 37 °C in the dark.

DOI: 10.1021/acs.jmedchem.8b01994
J. Med. Chem. 2019, 62, 1657−1668

Prior to flow cytometry analysis, cells were subsequently washed and resuspended in 1 mL of PBS. The fluorescence intensity of phosphohistone H2A.X (Ser139) antibody coupled with secondary antibody (FL1-H channel) and DHE (FL2-H channel) were measured on CyFlow Space flow cytometer (Partec, Münster, Germany). A minimum of 10 000 events were assayed for each sample.

DDR Studies. MCF7 cells were incubated overnight in adherent 60 mm culture dish (700 000 cells per dish) and then pretreated with 10 μM compound **5** or **pcm** for 30 min. Treatment with 10 μM protoapigenone was used as positive control. After this, they were exposed to UV irradiation (10 J/m^2) in the following 1 h to induce DDR. Protein collection and western blot assays were performed in accordance with the method described by our previous study.[19] Proteins of the cells were extracted with lysis buffer (1 mM EDTA, 10 mM tris(hydroxymethyl)aminomethane, pH 7.5, 0.5% NP-40, 10% glycerol, and 420 mM NaCl) supplemented with a cocktail of protease and phosphatase inhibitor (Roche Applied Science) and 1 mM DL-dithiothreitol. After sodium dodecyl sulfate-polyacrylamide gel electrophoresis, the separated proteins in the gel were electrophoretically transferred to nitrocellulose membranes. The membranes with the transferred proteins were detected using specific primary antibodies followed by horseradish peroxidase-coupled secondary antibodies (Jackson ImmunoResearch) and then recognized by enhanced chemiluminescence reagent (Millipore). Images were captured with a LAS-4000 luminescent image analyzer system (Fujifilm). The primary antibodies against Chk1-S345 and Chk2-T68 were purchased from Cell Signaling Technology (Danvers, USA); Chk1, Chk2, and β-actin were purchased from Santa Cruz. The β-actin expression served as an internal control.

Hydroxyl Radical-Scavenging Activity. The $^{\bullet}$OH-scavenging capacity of the investigated compounds (**pcm**, and NXY-059 as positive control) were performed by measuring the inhibition of damage to 2-deoxy-D-ribose by Fenton reaction.[38] Assays were carried out in 50 mM 3-(*N*-morpholino)propanesulfonic acid buffer, pH 6.0, containing 2.8 μM 2-deoxy-D-ribose, and increasing concentrations (0.002−5 mM) of samples to which 0.2 μM H_2O_2 and 1.5 μM $FeSO_4$ were added to start the reaction (in total volume of 280 μL). Then, after 3 min of incubation at 37 °C, during which period of time $^{\bullet}$OH formation was linear, TBA reactivity was developed by heating at 100 °C for 15 min after adding 400 μL of a mixture containing 15% (w/v) trichloroacetic acid, 0.25 M HCl, 0.325% (w/v) TBA, and 0.06 M NaOH. The resulting chromogens were measured at a wavelength of 532 nm against appropriate blanks.[39]

Combination Assay on the Cytotoxicity of pcm and H_2O_2. A checkerboard microplate method was applied to study the interaction between **pcm** and H_2O_2 concerning their cytotoxicity on MCF7 cells. Cells (1×10^4) were seeded to each well in a 96-well plate. The plates were incubated at 37 °C for 24 h. Standard solution of H_2O_2 (Sigma-Aldrich) and **pcm** were stored at −20 °C until use. The stock solutions and serial twofold dilutions of each drug were prepared according to the recommendations of several fix **pcm** vs H_2O_2 ratios to testing. **pcm** was serially diluted along the ordinate, while H_2O_2 was diluted along the abscissa. A total volume of 100 μL (including **pcm** and H_2O_2) was distributed into each well of the microdilution plates. The plates were incubated at 37 °C for 48 h, and then MTT solution was added to each well. After incubation at 37 °C for 4 h, the MTT-containing medium was removed, and 100 μL of DMSO was added to dissolve the formazan crystals. Cell viability was determined by measuring the optical density values (absorbance) of the chromogenic product at 550 nm with an enzyme-linked immunosorbent assay reader (Thermo Multiskan Ascent). Three plates were prepared on three different days, and averages of these three replicates were utilized to calculate the combination index (CI) values at several fix **pcm** vs H_2O_2 ratios by using the CalcuSyn software.

In Silico Calculations. Calculations were performed with the Gaussian09 package (Rev. A). Ground-state geometries were optimized using the B3P86 functional that has been shown to properly reproduce thermodynamics of polyphenol oxidative processes. The double-ζ basis set 6-31+G(d,p) was used to describe C-, O-, and H-atoms. Calculations were performed including solvation polarization effects by using conductor-like polarizable continuum model. Frequency calculations were performed to ensure that the obtained geometries were in the global minimum of the potential energy surface, as pictured by the absence of any imaginary frequency. Mulliken spin density visualization has been carried out using the VMD program.

■ ASSOCIATED CONTENT

Supporting Information

The Supporting Information is available free of charge on the ACS Publications website at DOI: 10.1021/acs.jmedchem.8b01994.

Experimental description of the stability test of **pcm** with ccH_2O_2 (30%) and HPLC−PDA chromatogram taken after 92 h; experimental description, HPLC−PDA, and LC−MS DAD1-EWC fingerprints of Fenton reaction of **pcm**, confirming the formation of compound **5**; atomic numbering and NMR signal assignment for compounds **1**−**5**; and molecular formula strings (PDF)
(CSV)

■ AUTHOR INFORMATION

Corresponding Author

*E-mail: hunyadi.a@pharm.u-szeged.hu. Phone: +36 62 546456. Fax: +36 62 545704.

ORCID

Milica Pesic: 0000-0002-9045-8239
Attila Hunyadi: 0000-0003-0074-3472

Present Address

††Synthetic Systems Biology Unit, Institute of Biochemistry, Biological Research Centre, Temesvári krt. 62, 6726 Szeged, Hungary.

Author Contributions

◆L.F., F.D.M., and C.-Y.K. contributed equally.

Notes

The authors declare no competing financial interest.

■ ACKNOWLEDGMENTS

This work was funded by the National Research, Development and Innovation Office, Hungary (NKFIH; K119770). Ministry of Human Capacities, Hungary grant 20391-3/2018/FEKUSTRAT is acknowledged. P.T. was funded by the Czech Science Foundation (P208/12/G016) and National Program of Sustainability I from the Ministry-of-Youth, Education and Sports of the Czech Republic (LO1305). A.H. was supported by the UNKP-18-4 New National Excellence Program of the Ministry of Human Capacities, by a Short-Term Scientific Mission (STSM) Grant from COST Action CM1407 "challenging organic syntheses inspired by nature—from natural products chemistry to drug discovery", by the János Bolyai fellowship of the Hungarian Academy of Sciences, and by the Kálmán Szász Prize. F.D.M. and P.T. thank CALI "CAlcul en LImousin" for computational resources as well as Nouvelle Aquitaine region for financial support. The authors acknowledge a bilateral mobility grant from the Hungarian Academy of Sciences and the Ministry of Science and Technology, Taiwan (MOST 107-2911-I-037-502).

■ ABBREVIATIONS

pcm, *p*-coumaric acid methyl ester; **cm**, caffeic acid methyl ester; **fm**, ferulic acid methyl ester; GI_{50}, 50% growth inhibitory concentration; PIFA, phenyliodine bis(trifluoroacetate); BCRP,

DOI: 10.1021/acs.jmedchem.8b01994
J. Med. Chem. 2019, 62, 1657−1668

breast cancer resistance protein; SEM, standard error of mean; MTT, 3-(4,5-dimethylthiazol-2-yl)-2,5-diphenyltetrazolium bromide; H2A.X, histone 2A.X; ATR, ataxia telangiectasia and Rad3-related kinase; ATM, ataxia telangiectasia mutated kinase; FA, Fanconi anemia; DSBs, DNA double-strand breaks; DPPH, 2,2-diphenyl-1-picrylhydrazyl; ABTS, 2,2′-azino-bis(3-ethylbenzothiazoline-6-sulphonic acid); 95% C.I., 95% confidence interval; CI, combination index; CI_{avg}, weighted average CI value; PDA, photometric diode array; SET, single-electron transfer; SPE, solid-phase extraction; HAT, hydrogen atom transfer; BDE, bond dissociation enthalpy; ACN, acetonitrile; PIDA, phenyliodine diacetate; DMEM, Dulbecco's modified Eagle's medium; FBS, fetal bovine serum; AV, annexin-V-FITC; PI, propidium iodide; DHE, dihydroethidium; PBS, phosphate-buffered saline; DDR, DNA damage response; HRP, horseradish peroxidase; ECL, enhanced chemiluminescence; MOPS, 3-(*N*-morpholino)propanesulfonic acid; TBA, thiobarbituric acid; C-PCM, conductor-like polarizable continuum model

REFERENCES

(1) El-Seedi, H. R.; El-Said, A. M. A.; Khalifa, S. A. M.; Göransson, U.; Bohlin, L.; Borg-Karlson, A.-K.; Verpoorte, R. Biosynthesis, natural sources, dietary intake, pharmacokinetic properties, and biological activities of hydroxycinnamic acids. *J. Agric. Food. Chem.* **2012**, *60*, 10877−10895.

(2) Chen, J. H.; Ho, C.-T. Antioxidant activities of caffeic acid and its related hydroxycinnamic acid compounds. *J. Agric. Food Chem.* **1997**, *45*, 2374−2378.

(3) Razzaghi-Asl, N.; Garrido, J.; Khazraei, H.; Borges, F.; Firuzi, O. Antioxidant properties of hydroxycinnamic acids: a review of structure-activity relationships. *Curr. Med. Chem.* **2013**, *20*, 4436−4450.

(4) Teixeira, J.; Gaspar, A.; Garrido, E. M.; Garrido, J.; Borges, F. Hydroxycinnamic acid antioxidants: an electrochemical overview. *Biomed. Res. Int.* **2013**, *2013*, 251754.

(5) Rao, C. V.; Desai, D.; Simi, B.; Kulkarni, N.; Amin, S.; Reddy, B. S. Inhibitory effect of caffeic acid esters on azoxymethane-induced biochemical changes and aberrant crypt foci formation in rat colon. *Cancer Res.* **1993**, *53*, 4182−4188.

(6) Xiao, H.; Parkin, K. L. Isolation and identification of potential cancer chemopreventive agents from methanolic extracts of green onion (Allium cepa). *Phytochemistry* **2007**, *68*, 1059−1067.

(7) Pieters, L.; Van Dyck, S.; Gao, M.; Bai, R.; Hamel, E.; Vlietinck, A.; Lemière, G. Synthesis and biological evaluation of dihydrobenzofuran lignans and related compounds as potential antitumor agents that inhibit tubulin polymerization. *J. Med. Chem.* **1999**, *42*, 5475−5481.

(8) Apers, S.; Paper, D.; Bürgermeister, J.; Baronikova, S.; Van Dyck, S.; Lemière, G.; Vlietinck, A.; Pieters, L. Antiangiogenic activity of synthetic dihydrobenzofuran lignans. *J. Nat. Prod.* **2002**, *65*, 718−720.

(9) Basini, G.; Spatafora, C.; Tringali, C.; Bussolati, S.; Grasselli, F. Effects of a ferulate-derived dihydrobenzofuran neolignan on angiogenesis, steroidogenesis, and redox status in a swine cell model. *J. Biomol. Screen.* **2014**, *19*, 1282−1289.

(10) Yin, S.-Y.; Jian, F.-Y.; Chen, Y.-H.; Chien, S.-C.; Hsieh, M.-C.; Hsiao, P.-W.; Lee, W.-H.; Kuo, Y.-H.; Yang, N.-S. Induction of IL-25 secretion from tumour-associated fibroblasts suppresses mammary tumour metastasis. *Nat. Commun.* **2016**, *7*, 11311.

(11) Kita, Y.; Tohma, H.; Hatanaka, K.; Takada, T.; Fujita, S.; Mitoh, S.; Sakurai, H.; Oka, S. Hypervalent iodine-induced nucleophilic substitution of para-substituted phenol ethers. Generation of Cation Radicals as Reactive Intermediates. *J. Am. Chem. Soc.* **1994**, *116*, 3684−3691.

(12) Urbaniak, A.; Molski, M.; Szeląg, M. Quantum-chemical calculations of the antioxidant properties of trans-*p*-coumaric acid and trans-sinapinic acid. *Comp. Methods Sci. Technol.* **2012**, *18*, 117−128.

(13) Canevali, C.; Orlandi, M.; Pardi, L.; Rindone, B.; Scotti, R.; Sipila, J.; Morazzoni, F. Oxidative degradation of monomeric and dimeric phenylpropanoids: reactivity and mechanistic investigation. *J. Chem. Soc., Dalton Trans.* **2002**, *0*, 3007−3014.

(14) Zhu, Y.; Zhang, L.-X.; Zhao, Y.; Huang, G.-D. Unusual sesquiterpene lactones with a new carbon skeleton and new acetylenes from *Ajania przewalskii*. *Food Chem* **2010**, *118*, 228−238.

(15) Chuang, T.-H.; Chan, H.-H.; Wu, T.-S.; Li, C.-F. Chemical constituents and biological studies of the leaves of *Grevillea robusta*. *Molecules* **2011**, *16*, 9331−9339.

(16) Atta-ur-Rahman; Shabbir, M.; Ziauddin Sultani, S.; Jabbar, A.; Choudhary, M. I. Cinnamates and coumarins from the leaves of *Murraya paniculata*. *Phytochemistry* **1997**, *44*, 683−685.

(17) Hunyadi, A.; Martins, A.; Danko, B.; Chang, F. R.; Wu, Y. C. Protoflavones: a class of unusual flavonoids as promising novel anticancer agents. *Phytochem. Rev.* **2013**, *13*, 69−77.

(18) Dankó, B.; Tóth, S.; Martins, A.; Vágvölgyi, M.; Kúsz, N.; Molnár, J.; Chang, F.-R.; Wu, Y.-C.; Szakács, G.; Hunyadi, A. Synthesis and SAR Study of Anticancer Protoflavone Derivatives: Investigation of Cytotoxicity and Interaction with ABCB1 and ABCG2 Multidrug Efflux Transporters. *ChemMedChem* **2017**, *12*, 850−859.

(19) Wang, H.-C.; Lee, A. Y.-L.; Chou, W.-C.; Wu, C.-C.; Tseng, C.-N.; Liu, K. Y.-T.; Lin, W.-L.; Chang, F.-R.; Chuang, D.-W.; Hunyadi, A.; Wu, Y.-C. Inhibition of ATR-dependent signaling by protoapigenone and its derivative sensitizes cancer cells to interstrand cross-link-generating agents *in vitro* and *in vivo*. *Mol. Cancer Ther.* **2012**, *11*, 1443−1453.

(20) Stanković, T.; Dankó, B.; Martins, A.; Dragoj, M.; Stojković, S.; Isaković, A.; Wang, H.-C.; Wu, Y.-C.; Hunyadi, A.; Pešić, M. Lower antioxidative capacity of multidrug-resistant cancer cells confers collateral sensitivity to protoflavone derivatives. *Cancer Chemother. Pharmacol.* **2015**, *76*, 555−565.

(21) Kastan, M. B.; Bartek, J. Cell-cycle checkpoints and cancer. *Nature* **2004**, *432*, 316−323.

(22) Chen, C. C.; Kennedy, R. D.; Sidi, S.; Look, A. T.; D'Andrea, A. CHK1 inhibition as a strategy for targeting Fanconi Anemia (FA) DNA repair pathway deficient tumors. *Mol. Cancer* **2009**, *8*, 24.

(23) Cole, K. A.; Huggins, J.; Laquaglia, M.; Hulderman, C. E.; Russell, M. R.; Bosse, K.; Diskin, S. J.; Attiyeh, E. F.; Sennett, R.; Norris, G.; Laudenslager, M.; Wood, A. C.; Mayes, P. A.; Jagannathan, J.; Winter, C.; Mosse, Y. P.; Maris, J. M. RNAi screen of the protein kinome identifies checkpoint kinase 1 (CHK1) as a therapeutic target in neuroblastoma. *Proc. Natl. Acad. Sci. U.S.A.* **2011**, *108*, 3336−3341.

(24) Brooks, K.; Oakes, V.; Edwards, B.; Ranall, M.; Leo, P.; Pavey, S.; Pinder, A.; Beamish, H.; Mukhopadhyay, P.; Lambie, D.; Gabrielli, B. A potent Chk1 inhibitor is selectively cytotoxic in melanomas with high levels of replicative stress. *Oncogene* **2012**, *32*, 788−796.

(25) Kuo, L. J.; Yang, L. X. Gamma-H2AX - a novel biomarker for DNA double-strand breaks. *In Vivo* **2008**, *22*, 305−309.

(26) Kwon, Y. S.; Kim, C. M. Antioxidant constituents from the stem ofSorghum bicolor. *Arch. Pharm. Res.* **2003**, *26*, 535−539.

(27) Kiliç, I.; Yeşiloğlu, Y. Spectroscopic studies on the antioxidant activity of *p*-coumaric acid. *Spectrochim. Acta, Part A* **2013**, *115*, 719−724.

(28) Fong, J. J.; Rhoney, D. H. NXY-059: review of neuroprotective potential for acute stroke. *Ann. Pharmacother.* **2006**, *40*, 461−471.

(29) Balogh, G. T.; Vukics, K.; Könczöl, Á.; Kis-Varga, Á.; Gere, A.; Fischer, J. Nitrone derivatives of trolox as neuroprotective agents. *Bioorg. Med. Chem. Lett.* **2005**, *15*, 3012−3015.

(30) Chou, T.-C. Theoretical basis, experimental design, and computerized simulation of synergism and antagonism in drug combination studies. *Pharmacol. Rev.* **2006**, *58*, 621−681.

(31) Trouillas, P.; Fagnère, C.; Lazzaroni, R.; Calliste, C.; Marfak, A.; Duroux, J.-L. A theoretical study of the conformational behavior and electronic structure of taxifolin correlated with the free radical-scavenging activity. *Food Chem* **2004**, *88*, 571−582.

(32) Trouillas, P.; Marsal, P.; Siri, D.; Lazzaroni, R.; Duroux, J.-L. A DFT study of the reactivity of OH groups in quercetin and taxifolin antioxidants: The specificity of the 3-OH site. *Food Chem* **2006**, *97*, 679−688.

DOI: 10.1021/acs.jmedchem.8b01994
J. Med. Chem. 2019, 62, 1657−1668

(33) Anouar, E.; Calliste, C. A.; Košinová, P.; Di Meo, F.; Duroux, J. L.; Champavier, Y.; Marakchi, K.; Trouillas, P. Free radical scavenging properties of guaiacol oligomers: a combined experimental and quantum study of the guaiacyl-moiety role. *J. Phys. Chem. A* **2009**, *113*, 13881−13891.
(34) Leopoldini, M.; Russo, N.; Toscano, M. The molecular basis of working mechanism of natural polyphenolic antioxidants. *Food Chem* **2011**, *125*, 288−306.
(35) Pastan, I.; Gottesman, M. M.; Ueda, K.; Lovelace, E.; Rutherford, A. V.; Willingham, M. C. A retrovirus carrying an MDR1 cDNA confers multidrug resistance and polarized expression of P-glycoprotein in MDCK cells. *Proc. Natl. Acad. Sci. U.S.A.* **1988**, *85*, 4486−4490.
(36) Pesic, M.; Markovic, J. Z.; Jankovic, D.; Kanazir, S.; Markovic, I. D.; Rakic, L.; Ruzdijic, S. Induced resistance in the human non small cell lung carcinoma (NCI-H460) cell line in vitro by anticancer drugs. *J. Chemother.* **2006**, *18*, 66−73.
(37) Mosmann, T. Rapid colorimetric assay for cellular growth and survival: application to proliferation and cytotoxicity assays. *J. Immunol. Methods* **1983**, *65*, 55−63.
(38) Mathew, S.; Abraham, T. E. In vitro antioxidant activity and scavenging effects of *Cinnamomum verum* leaf extract assayed by different methodologies. *Food Chem. Toxicol.* **2006**, *44*, 198−206.
(39) Tadolini, B.; Cabrini, L. The influence of pH on OH scavenger inhibition of damage to deoxyribose by Fenton reaction. *Mol. Cell. Biochem.* **1990**, *94*, 97−104.

DOI: 10.1021/acs.jmedchem.8b01994
J. Med. Chem. 2019, 62, 1657−1668